Results in Physics 17 (2020) 103025

Contents lists available at ScienceDirect

Results in Physics

journal homepage: www.elsevier.com/locate/rinp

Synthesis, optical, thermal, electric properties and impedance spectroscopy studies on P(VC-MMA) of optimized thickness and reinforced with MWCNTs

Adel M. El Sayed

Department of Physics, Faculty of Science, Fayoum University, Fayoum 63514, Egypt

ARTICLE INFO

Keywords:
P(VC/MMA) nanocomposites
Bandgap engineering
Wrinkle structure
Thermal stability
Ac and dc conductivity
Nyquist plots

ABSTRACT

The synthesis of polymeric blends and nanocomposites with improved physical properties has attracted increasing attention worldwide, for its practical and technological applications. The present study aims to tune the physical properties of thermoplastic polyvinyl chloride (PVC) and polymethyl methacrylate (PMMA) blends by adjusting the film thickness and loading with multiwall carbon nanotubes (MWCNTs). To this end, P(VC/MMA) films of thickness in the range 36.4–204 μm and P(VC/MMA)/MWCNTs films were prepared using solution casting. A scanning electron microscope (SEM) and Fourier transform infrared spectroscopy (FTIR) were used to investigate the films morphology and cross-sectional area and the vibrational properties, respectively. UV–vis measurements demonstrated that the transmittance spectra and absorption index were significantly affected by the film thickness and fillers content ratio. Moreover, both the direct and indirect optical bandgap increased with increasing thickness and decreased with increasing MWCNTs content inside P(VC/MMA) films. Further, thermogravimetric analysis (TGA) and differential scanning calorimetric (DSC) showed that the films exhibit thermal stability in the temperature range of 179–230 °C, and the melting temperature and degree of crystallinity increased with increasing thickness and decreased after doping with MWCNTs. The influences of film thickness and MWCNTs on the refractive index, dielectric constant, dielectric modulus, ac conductivity, impedance, and Nyquist plots have been discussed, along with the induced capacitance nature of the samples. Consequently, it was ascertained that the observed improvement in the optical properties and ac conductivity make these blends and nanocomposites suitable for optical devices and dielectric applications.

Introduction

Recently, the fabrication of polymeric blends and nanocomposites has attracted an increased amount of attention worldwide, as an emerging low-cost technology. With the incorporation of a small number of nano-fillers, the development of electrically conductive networks can be undertaken efficaciously in the insulating polymer. Notably, this is in addition to the improvement in optical and thermal properties [1,2]. With specific thicknesses, layers of conductive polymer nanocomposites are used to manufacture electromagnetic interference (EMI) shielding applications, as well as cable sheathing for the supply of high voltage applications [3]. Additionally, these materials are used for optical devices fabrication as well as dielectric materials to develop capacitors owing to their high dielectric permittivity and refractive indices [4].

PVC, $(CH_2–CH–Cl)_n$, and oxygen-containing hydrophilic PMMA, $(CH_2 = C[CH_3]CO_2CH_3)_n$, are extensively used thermoplastics owing to their low-cost and hygienic properties [4]. PVC is used in the plastics and microelectronic industry (for example, cables and wires insulation) in wake of its excellent corrosion and abrasion resistance, low combustibility, electrical insulation, withstanding the conditions of extreme heat and radiations, and mechanical stability that arises from the dipole–dipole interaction between H and Cl atoms [5–7]. According to Feng et al. [8] the tensile strength and density of PVC/wood fiber composite has increased by 112% and decreased by 52.55%, respectively, after modification by 15% NaOH solution. On the other hand, PMMA is used in LCD as light guidance panels and transparent covers for electronic devices due to its transparency and light-weight [5,9]. PMMA is a non-crystalline polymer of melting point ~130 °C, that is clinically accepted bio/mechanical material used for facial prostheses, as well as tooth restorative materials [10,11]. Additionally, PMMA finds applications for EMI shielding, due to its strong interfacial adhesion with the nanofillers [6]. Correspondingly, Kim et al. [12] have used PVA/PMMA copolymer as a structure-directing agent in the synthesis of mesoporous TiO_2, SiO_2, Al_2O_3, ZrO_2, Fe_2O_3, SnO_2, and ZnO films with both high porosity and good interconnectivity.

Using the phase inversion method, Bhran et al. [13] prepared PVC/PVP porous membranes that are useful for sea and brackish water

E-mail address: ams06@fayoum.edu.eg.

https://doi.org/10.1016/j.rinp.2020.103025
Received 5 January 2020; Received in revised form 18 February 2020; Accepted 24 February 2020
Available online 02 March 2020

distillation. Blending poly (butyl methacrylate) or PMMA with PVC yielded a blend of conductivity of 1.1×10^{-5} or 2.79×10^{-6} S/cm, respectively, with significant mechanical and thermal stability [7,14]. Importantly, incorporation of the inorganic nano-filler has been shown to be an efficacious method for improving the overall performance of PVC [15,16]. According to Arunkumar et al. [17], the addition of Al_2O_3 nanoparticles (NPs) till 10 wt% into the PVC/polybutyl methacrylate / $LiClO_4$) creates electrolyte of porous structure with enhanced ionic conductivity from 0.7×10^{-3} to 9.3×10^{-3} S/cm. The PVC is an H^+ donor, whereas PMMA is an H^+ acceptor. Thus, the blend of PVC and PMMA is expected to create a strong hydrogen bonding between the H atom of PMMA and Cl atom of PVC. Some investigators have remarked that PVC and PMMA are miscible up to 60 wt% of PMMA [18]. However, others [19] reported that the PMMA ratio should be $\leq$40 wt% in order to get a valid miscible P(VC/MMA) for electronic and engineering applications. Furthermore, TGA and DSC analysis demonstrated that the existence of 70 wt% of PVC enhances the thermal stability and miscibility of P(VC/MMA) blend [5].

Introducing GeO_2 NPs into the P(VC/MMA) blend was found to improve its thermal stability, dielectric constant and its EMI shielding properties [6]. The addition of PMMA and PMMA/ nano-sized SiO_2 was found to increase the tensile strength, Young's modulus, tear strength and thermal stability and decrease elongation at the break of PVC [20]. Due to the weak adhesion between the two components, adding $CaCO_3$ whiskers [16] or TiO_2 NPs [21] negatively affected the mechanical and thermal properties of PVC. However, these properties improved significantly by modifying $CaCO_3$ or TiO_2 with PMMA as a result of the enhanced interfacial adhesion. Also, the thermal, mechanical and electrochemical properties of 0.9PVC/0.1PMMA blend were improved after loading the blend with (1–5 wt%) CuO NPs [22]. Moreover, PMMA is often used as a compatibilizing agent for PVDF/NPs composite to act as a bridge between the fillers and PVDF chains [23].

Carbon nanotubes (CNTs) have a special electronic, chemical, thermal, mechanical properties, low-mass density, high flexibility, a very high surface area, and the aspect ratio, and can produce massive interface in the polymer nanocomposites [3,24–26]. Kumar et al. [26] reported that the MWCNTs inside polyaniline serve as conducting bridges that connect the polymer domains improving its electrical conductivity and EMI shielding. According to Wu et al. [27] MWCMTs coated by amorphous carbon and then decorated by magnetic nanoparticles (MWCNTs@C@Fe/α-Fe_2O_3) presented an excellent wideband electromagnetic absorber at thickness ~1 mm. Kim et al. [10] doped PMMA with MWCNTs for preventing the microbe-induced complications. Also, it was reported that MWCNTs induce more irregular order (i.e. decreasing the films' crystallinity of polyurethane/PVC), better homogeneous dispersion and improved the electrical conductivity significantly compared with single-walled carbon nanotubes (SWCNTs) [28]. Although the polymer/MWCNTs composites have remarkable properties, the tendency of the CNTs to aggregate (owing to the high intrinsic van der Waals forces) limits their application. Thus, the optimized content of CNTs usually introduced in the composite membrane is very low, even when functionalized by oxidation processes [23].

The aims of the present work; i) to study the influence of thickness on the physical properties of PVC (75%)/PMMA (25%) blend prepared by solution casting. ii) study the influence of MWCNTs doping ratio on the properties of P(VC/MMA) of optimized thickness. The influences of films thickness and MWCNTs content on the morphology, structure, optical, thermal, electric properties and impedance spectroscopy of P (VC/MMA) blend were investigated, discussed, and compared with those of similar compounds, as no data are available in the literature concerning the effect of thickness on the blend performance.

Experimental

Materials and preparation

PVC, Polymer Lab., UK, and PMMA of MW = 350,000 g/mole, Acros Organics, were used for the blend preparation. Tetrahydrofuran (THF), Aldrich, Germany, was used as the solvent. MWCNTs, from the Egyptian Petroleum Research Institute (EPRI), purity $>$ 90%, density = 1.7 g/cm^3, their lengths varied between 100 nm up to few μm, crystallite size $<$ 40 nm. XRD and HR-TEM images are shown in Fig. S1. PVC/PMMA blends with (75%/25%) constant ratio were prepared by mixing (0.375 g PVC + 0.125 g PMMA) in 25 ml THF, (0.75 g PVC + 0.25 g PMMA) in 50 ml THF, and (1.5 g PVC + 0.5 g PMMA) in 100 ml THF, respectively to get films with different thicknesses. The dissolutions carried out, in beakers with tightly closed orifices to prevent the volatilization of the solution, with continuous stirring for 2 h at RT till the complete dissolution of the blend. The mixtures were cast into glass Petri dishes of 11 cm in diameter and suitable depth and put in the air for solvent evaporation at room temperature (RT). For some reason, mentioned in the discussion section, the mixture (0.75 g PVC + 0.25 g PMMA) was chosen for nanocomposites preparation. To this solution, 0.25, 0.50 and 1.0 wt% of MWCNTs were weighted and mixed. Additional time (1.0 h) for magnetic stirring combined with sonication for 20.0 min to ensure the uniform distribution and dispersion of the fillers inside the blend matrix. The basic steps of the preparation procedures are shown in Fig. 1. Care was taken to obtain homogenous blends and nanocomposite films. To remove moisture and the residual solvent, the obtained films were dried at 50 °C in a vacuum oven for 2.0 h.

Characterization

The surface morphology of the blends and nanocomposite films, their cross-section, and thicknesses were investigated by SEM, Inspect S, FEI, Netherlands, by using an accelerating voltage of 20 kV. The surface of the samples was coated with a ~ 3.5 nm gold layer to decrease the sample charging effects as a result of the e-beam. Fourier transform infrared spectroscopy (FTIR) to study the vibrational properties and functional groups in P(VC/MMA) blends and their nanocomposites were done by using (JASCO, FT/IR-6200) in the wavenumber range 400–4000 cm^{-1}. The optical spectra were recorded at RT using the UV-3600/UV–VIS-NIR Shimadzu spectrophotometer with an accuracy of ± 0.2 nm, in the wavelength range of 200–1750 nm. Thermogravimetric analysis (TGA) was done by TGA (Q50, TA instruments). About 5.6 mg of each sample was heated from RT to 750 °C at a rate of 10 °C/min under an inert N_2 atmosphere. The differential scanning calorimetric (DSC) was carried out by DSC; Shimadzu DSC-60 in the temperature range RT − 750 °C with a heating rate of 10 °C/min in an N_2 atmosphere. Before use, the instrument was calibrated with Aluminum oxide standard. The accuracy of the heat flow was ± 0.01 mW. Dielectric properties and impedance spectroscopy (ε', ε'', tan δ, Z' and Z'') were recorded by a Hikoi (Ueda, Nagano, Japan) model 3532 High Tester LCR, in the frequency range 1.0 Hz to 3.0 MHz, with capacitance measurement accuracy on the order of 1×10^{-4} pF, at RT.

Results and discussion

SEM analysis and FTIR spectroscopy

Fig. 2(a–c) shows the cross-sectional area of pure blend films prepared with different thicknesses. The average thickness of these films is ~36.4, 91.4, and 204 μm, as measured by SEM. One can note that there is a good homogeneity between PVC and PMMA polymers, i.e. no phase separation can be noticed. With increasing the film's thickness beyond 36.4 μm, some voids are created inside the film of thickness 91.4 μm, and they appear clearly in the 204 μm thick film. These voids or pores

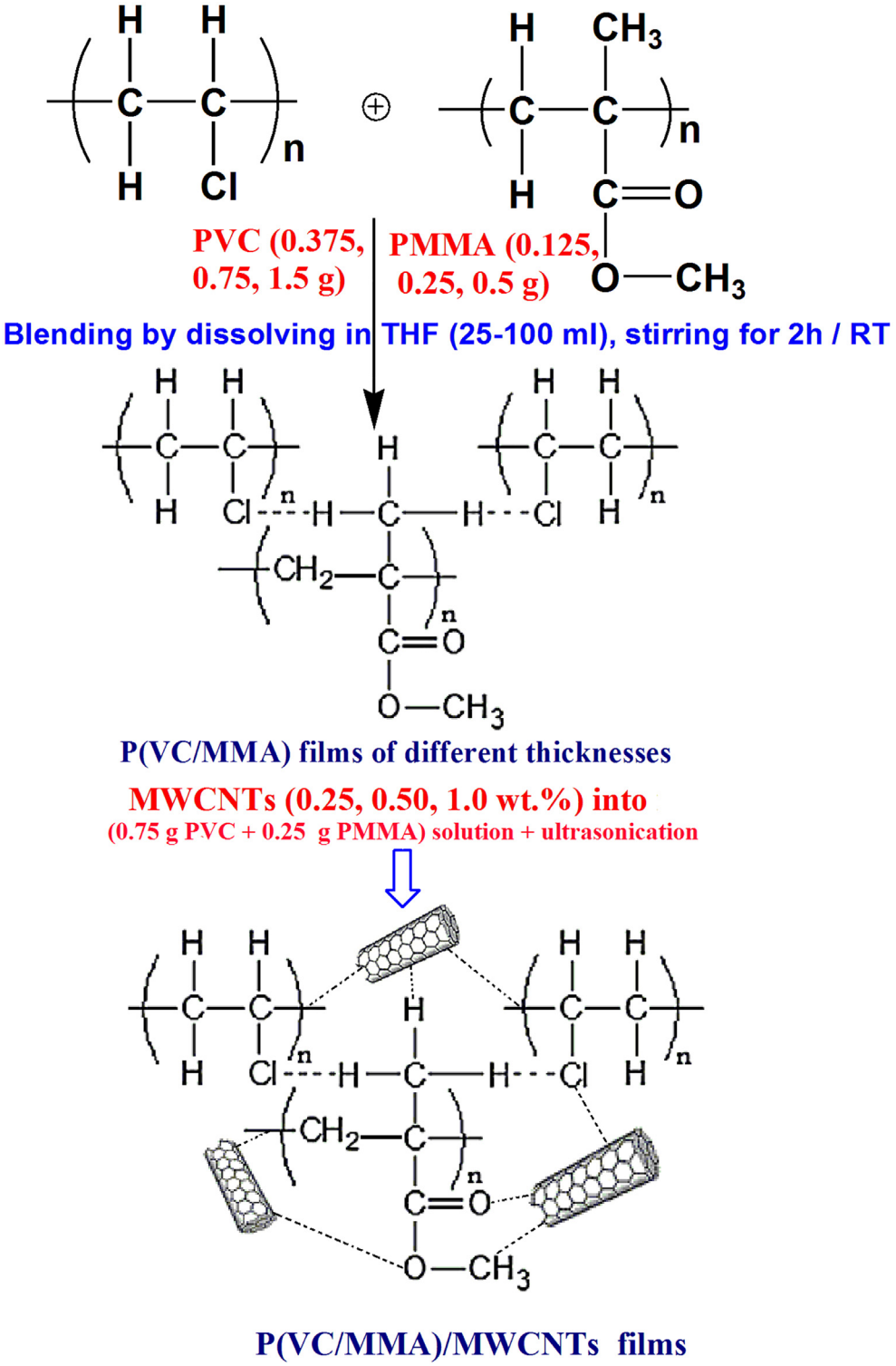

Fig. 1. . Preparation procedures and formation of bonds in P(VC/MMA) and P(VC/MMA)/MWCNTs.

aren't observed on the top surface of these films, Fig. 2 (d, e). Moreover, these two surfaces show a net-wrinkle structure that affected slightly by increasing the thickness from 91.4 to 204 μm. Creating pores inside the polymer films, in general, enhance their usability in the electrochemical applications by increasing the electrolyte uptake and the ionic conductivity [29]. The effect of MWCNTs at 0.25–1.0 wt% loading on the surface morphology of the P(VC/MMA) blend of medium thickness (91.4 μm) is seen clearly in Fig. 3(a–d). At a lower magnification compared to that used in Fig. 2 (d, e), the pristine film exhibits a fingerprint-like structure turned to be a wave-like morphology after loading with 0.25 and 0.50 wt% MWCNTs. The disappearance of the MWCNTs from the films' surface and inside the films after filling with 0.25 and 0.50 wt%, Fig. 3 (e, f), is due to the presence of MWCNTs in small ratios and the good dispersion of the fillers in the polymer matrix. This indicates that the blend made a strong interaction with the MWCNTs. Moreover, due to this interaction, the average film thickness of the films loaded with MWCNTs, Fig. 3 (e, f), is ~80.3 μm, which is less than that of the pure blend (91.4 μm). Additionally, it is seen in

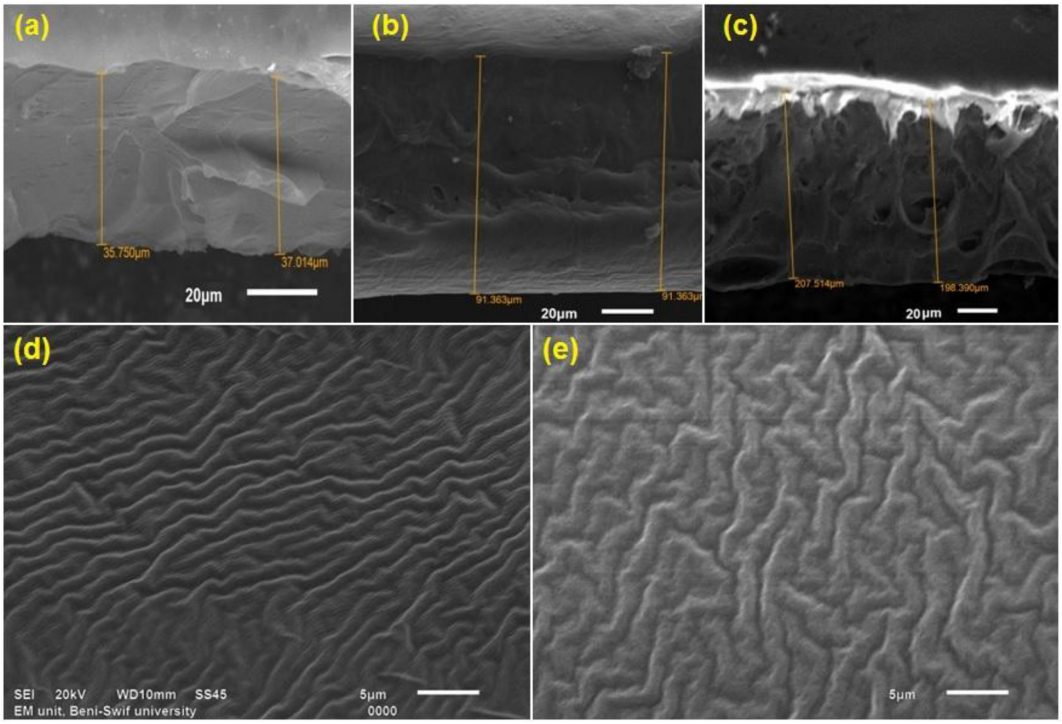

Fig. 2. . (a-c) cross-section of films with different thicknesses, (d, e) the top surfaces of 91.4 μm and 204 μm thick films.

Fig. 2(d, e) and Fig. 3(a–d), there is no division surfaces between PVC and PMMA in the pure blends or that doped with MWCNTs. This suggests the miscibility between the films' components at the molecular level. Similarly, Khutia and Joshi [19] reported that a well interconnecting network have been created between NiO NPs and the micropores in P(VC/MMA) at the lowest doping ratio of the fillers.

To investigate the influence of the film's thickness and MWCNTs content on the functional groups of P(VC/MMA), FTIR spectroscopy was done as shown in Fig. 4 (a, b). The band at 2925 cm^{-1} is owing to the stretching vibrations of C—H bonds. The band at ~1433 cm^{-1} is due to the wagging of methylene groups in PVC and/or owing to the asymmetric stretching of O–CH_3 group of PMMA [6,7]. The intensity of the 2925 and 1433 cm^{-1} bands are significantly improved with increasing both the films' thickness and MWCNTs content from 0.25 to 1.0 wt%. The weak band at 2347 cm^{-1} is assigned to CH_2 bending second overtone. The 1727 cm^{-1} characteristic peak is attributed to the C═O stretching vibration of the acrylate carboxyl group of PMMA and the weak peak at 1601 cm^{-1} is of the C═C conjugated stretching [5,11]. As can be noted, with increasing the films' thickness or MWCNTs content, the 1727 cm^{-1} band grown at the expense of the 1601 cm^{-1} one. The 1328 cm^{-1} band is originating from the overlapping of CH_2 wagging in PMMA and CH_2 deformation mode of PVC. This band is enhanced by increasing the films' thickness. The peak at 1245 cm^{-1} is assigned to the stretching vibration of C–H/–OCH_3 [5,6]. The band at 1151 cm^{-1} is due to C–O–C absorption of PMMA. Again, the intensity of this band increased with increasing thickness and MWCNTs content above 0.25 wt%. The characteristic absorption of C–C band appears at 1062 cm^{-1}. The bands at 961 and 847 cm^{-1} are of CH_2 rocking vibration [18]. The bands at 688 cm^{-1} and 617 cm^{-1} demonstrate the C–Cl bond of the isotactic and syndiotactic structure of PVC [6]. Increasing the bands intensity after increasing film thickness to 204 μm is logic and owing to the increased number of the functional groups in the path of IR radiation. A similar result was reported for CuO films [30]. Moreover, the intensity of most of P(VC-MMA) bands are decreased after loading with 1.0 wt% MWCNTs. This is attributed to the high surface energy and the huge tendency of CNTs to form bonds with the blend molecules, as shown in Fig. 1. These results confirm the influence of film thickness and the nano-fillers content on the vibrations of blend' functional groups and the interactions between the components of the nanocomposite films.

Optical characterization of the films

Fig. 5(a, b) shows the transmittance spectra of P(VC/MMA) blends and composite films. In the studied wavelength range, T% increases with increasing λ. The sharp increase in T% values in the region 200 – 300 nm is owing to the high energy of the incident photons which can excite a large number of the electrons from the valence band to the conduction band. Increasing the films' thickness from 36.4 to 204 μm leads to a large reduction in T%, for comparison, at $\lambda = 10^3$ nm, the T values of these films decrease from 78.4 to 27%. Also, loading MWCNTs with ratios between 0.0 and 1.0 wt%, decreases the T value from 62.7 to 18%, as listed in Table 1. Similarly, increasing the thickness of CuO material from 135 to 525 nm reduced T% from 80 to 58 [30]. Additionally, the observed reduction in T% with increasing the nanofillers' content is a legal result, where they act as scattering centers for the incident light.

Fig. 6 (a, b) shows the spectra of the absorption index, $k = \frac{\alpha\lambda}{4\pi}$, where the absorption coefficient $\alpha = absorption/film\ thickness\ (d)$. All films exhibit a sharp absorption edge in the region of 225–240 nm. The sharpness of this edge slightly decreased with increasing the film's thickness but increased with increasing MWCNTs content to 1.0 wt%. This may be due to the increased disorder in the blend matrix. The absorption band at ~283 nm seen in the spectra of all films is due to $\pi \rightarrow \pi^*$ transitions, arising from the unsaturated C═O and C═C bonds. As seen in the inset of Fig. 6 (b), another band at ~217 nm is owing to $n \rightarrow \pi^*$ transitions [31]. This band is created and enhanced only by increasing MWCNTs ratio in the blend. This result assures the interaction and complexation between the nano-fillers and the blend chains, as discussed in FTIR results. Additionally, the k values are very small (in the order of 10^{-4}), decreased with increasing the films' thickness but increased with increasing MWCNTs loading. This result illustrates the possibility of controlling the optical absorption of P(VC/MMA) films by adjusting their thickness and composition.

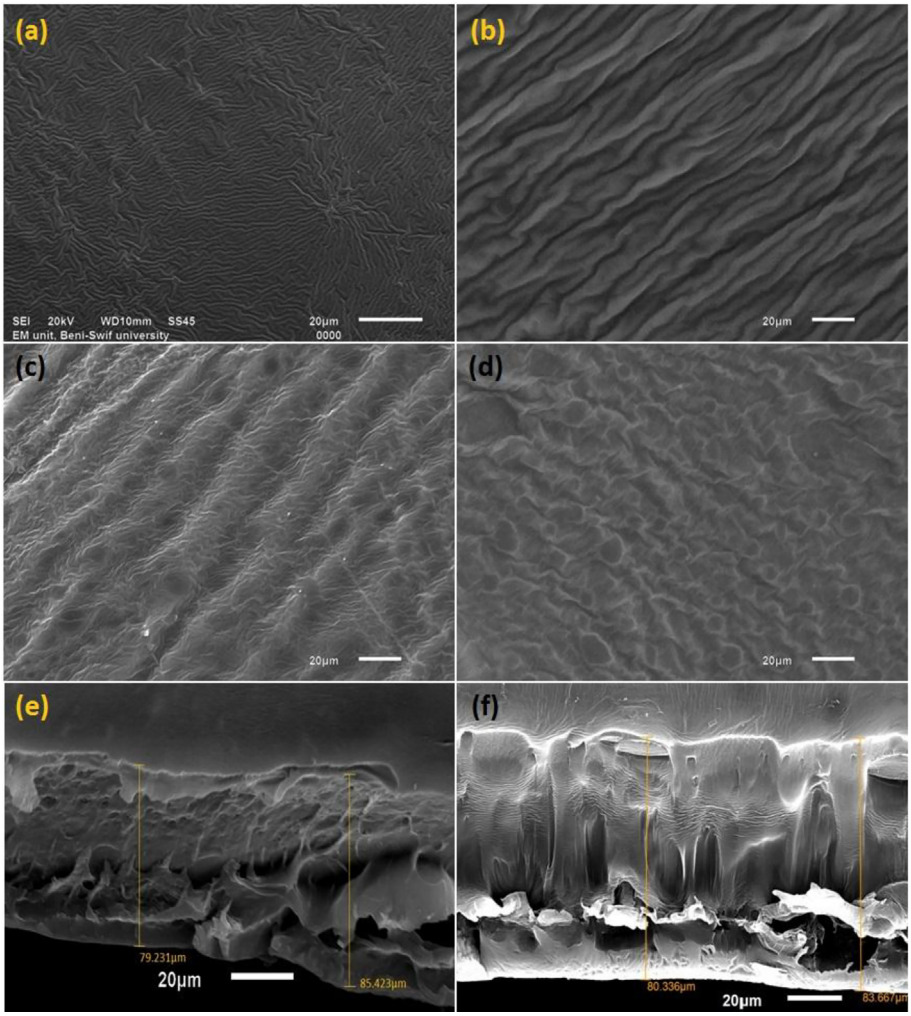

Fig. 3. . SEM analysis: top surface images of (a) pure PVC/PMMA blend and (b-d) blend loaded with 0.25%, 0.50%, and 1.0 wt% MWCNTs. (e, f) the cross-section of 0.25% and 0.50% MWCNTs films, respectively.

The electronic band structure and the type of allowed optical transitions can be checked applying the equation; $(m\alpha h\upsilon)^q = B(h\upsilon - E_g)$, where m is an integer, $h\upsilon$ is the photon energy, B is a constant, $q = 1/2$ and 2 for the indirect optical transition (E_g^{in}) and for the direct transition (E_g^{di}), respectively. For E_g^{di}, the highest of the valence band (VB) and the bottom of the conduction band (CB) lie at zero crystal momentum. Taking $m = 1$, the plotting of $(\alpha h\upsilon)^2$vs. $h\upsilon$and plotting of $(\alpha h\upsilon)^{1/2}$vs. $h\upsilon$, can yield the E_g^{di} and E_g^{in}, respectively, as shown in Fig. 7 (a, b) and in the insets of Fig. 7 (a, b), respectively. E_g^{di} and E_g^{in} values are obtained by extraplotting the straight-lines portion to $(\alpha h\upsilon)^2 = 0$ and $(\alpha h\upsilon)^{1/2} = 0$, respectively, and their values are listed in Table 1. The obtained results indicate that the bandgap of P(VC/MMA) blends can be easily controlled by adjusting the films' thickness and fillers' content. Increasing the thickness from 36.4 to 204 μm widened both E_g^{di} and E_g^{in} from 4.82 to 5.0 eV and from 3.9 to 4.7 eV, respectively. However, increasing fillers content from 0.0 to 1.0 wt% narrowed E_g^{di} and E_g^{in} from 5.0 to 4.63 eV and from 4.55 to 4.0 eV, respectively. Similarly, doping PVC/PVdF blend with 0.01% GO reduced its E_g^{in} from 5.0 to ~ 4.4 eV [15]. Increasing the film thickness increases the insulating properties and increasing MWCNTs improves the semiconducting character of P(VC/MMA) blends. The nature of 1D morphology and the uniform distribution of MWCNTs inside the blend matrix enable them to form 3D connected network structures that facilitate the charge transport process. The obtained results are the best compared with that reported for PMMA(80%)/PVdF(20%), as its E_g^{di} just reduced from 5.85 to 5.22 eV after loading ZnO NPs with the ratio of 20 wt%. [32].

Fig. 8 (a, b) shows the distribution of the films' refractive index (n), calculated using the relation: $n = \frac{1+\sqrt{R}}{1-\sqrt{R}}$ [33]. n shows anomalous dispersion in the UV region and normal dispersion in the longer wavelengths. Moreover, n value lies between 1.8 and 5, as listed in Table 1. Where it increases with increasing both the films' thickness and filler content. MWCNTs may act as scattering centers that reduce the light velocity in the nanocomposite films. Thereby increase n value in accordance with ($n = c/v$),where c and v are the velocity of light in the free space and in the material, respectively. The dispersion relation: $n^2 = \varepsilon_L - \left(\frac{e^2}{\pi c^2}\right)\left(\frac{N}{m^*}\right)\lambda^2$ [30], has been used to determine both the lattice dielectric constant ε_L and The ratio of carrier concentration to the electron effective mass $\left(\frac{e^2}{\pi c^2}\right)\left(\frac{N}{m^*}\right)$. The obtained results are tabulated in Table 1. With increasing films' thickness and MWCNTs content, ε_L increased significantly. Increasing $\left(\frac{e^2}{\pi c^2}\right)\left(\frac{N}{m^*}\right)$ from $8.50\text{x}10^{-7}$ to $4.45\text{x}10^{-6}$ nm^{-2} with increasing MWCNTs content is in agreement with decreasing E_g of the samples. Reducing the E_g and increasing n value after incorporation of MWCNTs was also reported for the PVA/PVP blend [24]. The obtained results illustrate that the prepared films are a candidate for designing high refractive index lenses or optical filters with a reasonable optical bandgap.

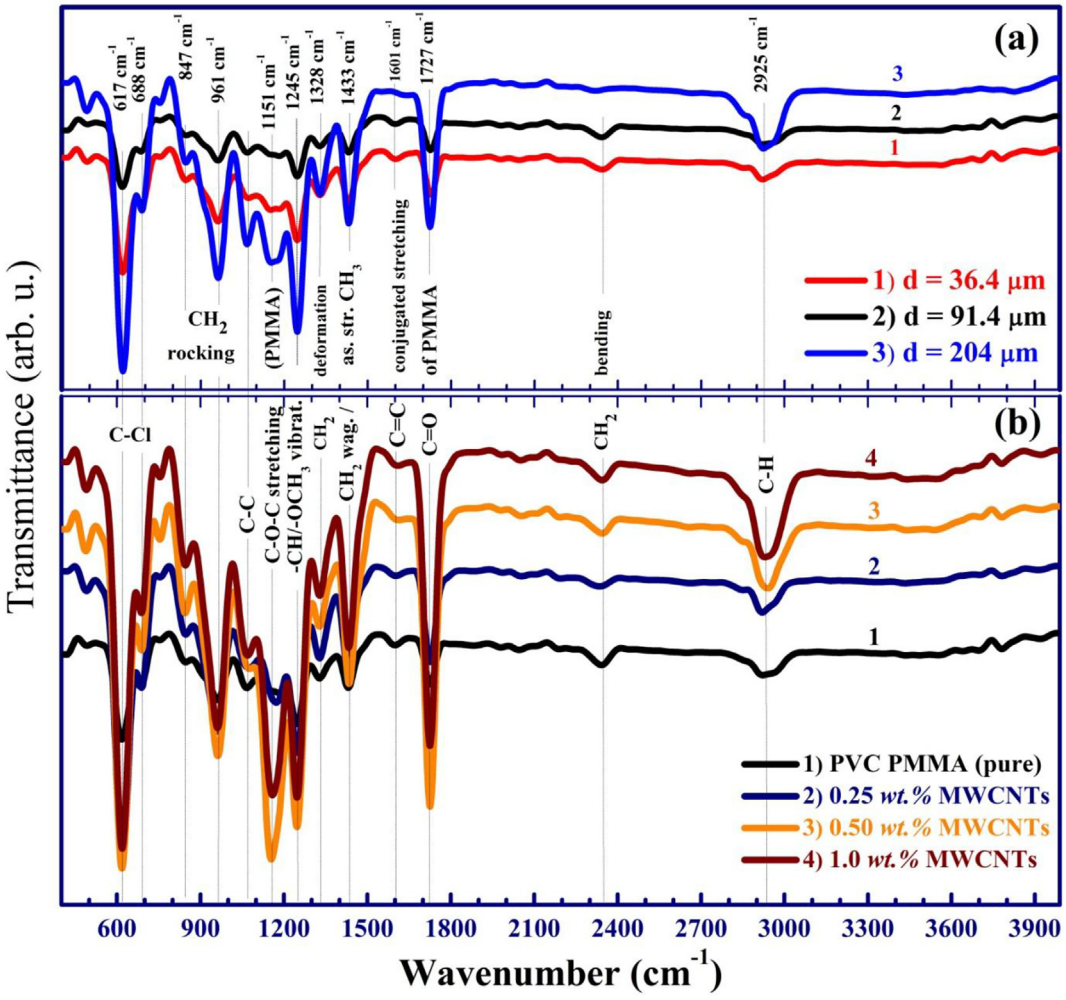

Fig. 4. . FTIR transmittance spectra of PVC/PMMA blend of (a) different thicknesses and (b) that loaded with 0.25 wt%, 0.50 wt% and 1.0 wt% MWCNTs.

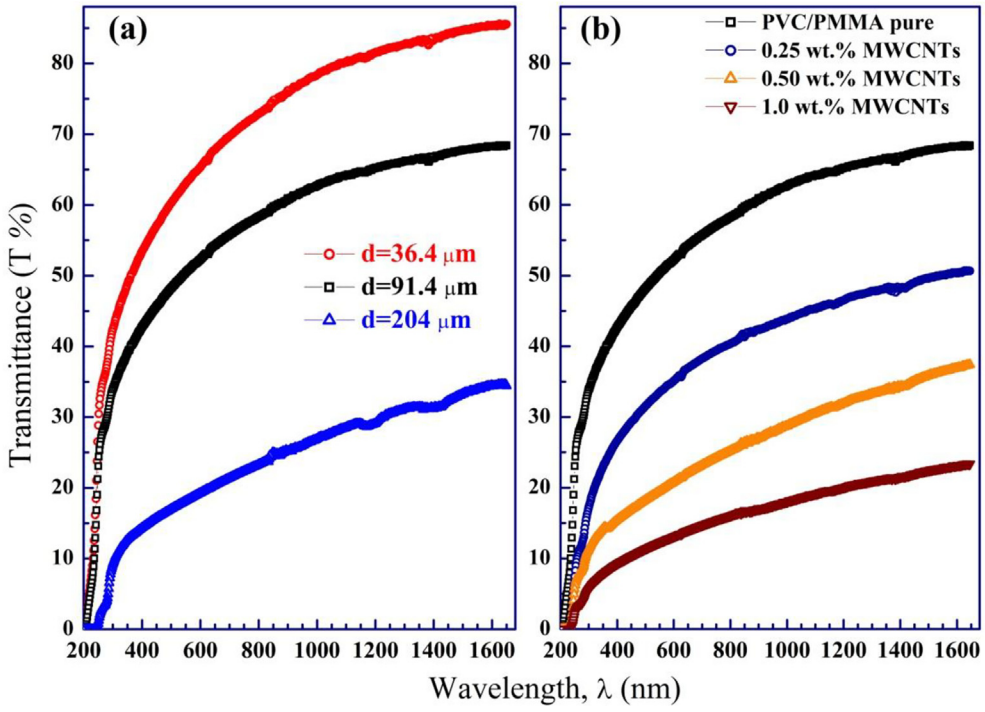

Fig. 5. . UV–vis transmittance spectra of the films.

Table 1
. Direct and indirect band gap (E_g), transmittance (T%) and refractive index (n) at λ = 700 nm, lattice dielectric constant ε_L and the ration of electron charge to effective mass $\left(\frac{e^2}{\pi c^2}\right)\left(\frac{N}{m^*}\right)$ for the PVC/PMMA blend prepared with different thicknesses and that loaded with MWCTNs.

Films		T% at 10^3 nm	E_g^{di}(eV)	E_g^{in}(eV)	*n* at 700 nm	ε_L	$\left(\frac{e^2}{\pi c^2}\right)\left(\frac{N}{m^*}\right)(nm)^{-2}$
Thickness effect	d = 36.4 μm	78.4	4.82	3.90	1.8	2.50	$8.23x10^{-7}$
	d = 91.4 μm	62.7	4.98	4.50	1.9	3.00	$2.46x10^{-7}$
	d = 204 μm	27.0	5.00	4.70	3.6	10.2	$2.70x10^{-6}$
Doping effect	PVC/PMMA	62.7	5.00	4.55	1.9	3.0	$8.50x10^{-7}$
	0.25% MWCNTs	43.9	4.95	4.35	2.4	4.8	$2.72x10^{-7}$
	0.50% MWCNTs	28.7	4.85	4.19	3.7	10.8	$3.19x10^{-6}$
	1.0% MWCNTs	18.0	4.63	4.00	5.0	20.2	$4.45x10^{-6}$

TGA and DSC analysis

TGA is a widely used technique for exploring the thermal stability of the organic compounds, where the weight loss W (%) of the material is recorded as a function of temperature. The TGA thermograms of P(VC/MMA) blends of different thicknesses and P(VC/MMA)/MWCNTs are shown in Fig. 9. The observed initial weight loss from RT (~22 °C) to 178 °C is due to the spread and dispersal of persistent THF, moisture, fluorine impurities, and CO/CO_2 evaporation [34]. Between 179 and 230 °C, the films show thermal stability, as the W (%) loss is negligible. This means that the onset decomposition temperature (T_O) the films ~230 °C. T_O for the blend with thickness 91.4 μm ~ 240 °C and the weight loss is ~ 9%. This means that at this thickness, the blend exhibits higher thermal stability. In the ranges, 231–285 °C and 385–490 °C, the second and the final decomposition occur for most of the films. This is attributed to the reduction of molecular weight (degradation) of the blend chains, the dehydrochlorination of PVC in the blend, and the degradation of unsaturated polymers, i.e. the cleavage backbone of the polymer [6,35]. Weight loss of the neat blend for the second stage of degradation is 52%. At T > 490 °C, the remaining weight is in the range 10–15 %, and is due to the residue char. Fig. S2(a–f) shows the DTG curves used to determine the maximum thermal degradation temperature (T_{max}), i.e. the temperature at which the maximum W (%) rate is reached. The obtained T_{max} values are listed in Table 2. The T_{max} decreased from 262 to 252 °C with increasing the film's thickness from 36.4 to 204 μm. Also, its values are in the range 255–261 °C, after loading with MWCNTs. This result means that loading MWCNTs accelerate the dehydrochlorination of PVC in the blend. Ayaz et al. [22] reported a T_{max} = 296 °C for PVC (90%)/PMMA (10%) blend that decreased to 270, 272 and 285 °C after mixing CuO NPs at ratios of 1, 5, and 7 wt%, respectively.

DSC is a thermal analysis technique used for describing the thermal transitions in the blends and composites, under a pre-controlled temperature profile at an inert atmosphere. Fig. 10 shows the DSC curves of P(VC/MMA) blends and P(VC/MMA)/MWCNTs in the temperature range RT − 450 °C. All the observed peaks are endothermic. The small peak in the range of 55–70 °C is assigned to the glass - rubber transition (T_g), owing to the micro- Brownian segmental motion of main chains. Another endothermic peak at about 279 °C for the thinner film (36.4 μm) shifted to 292 °C for the 204 μm thick film. This peak is attributed to the melting temperature (T_m) of the blends. After loading MWCNTs with 0.25 to 1.0 wt% ratios, T_m decreased from 289 to 280 °C. The third endothermic peak is in the temperature range 385–420 °C and is attributed to the decomposition temperature (T_d) of the blends. The values of T_m and T_d are also listed in Table 2. The DSC thermogram of P(VC/MMA) pure blend shows a single T_g indicating the miscibility of the blend components, confirming the SEM observation. The T_g values increased with increasing films' thickness and decreased with increasing MWCNTs content in the blend. This indicates that increasing the films' thickness hinders the segmental mobility of the amorphous regions in the blend. However, increasing MWCNTs ratio lead to less rigid segments and affect the orientation of crystals and the films' microstructure.

The decrease in T_m is an indication of the decrease in films' crystallinity. It further leads to the improvement in the segmental motion of the polymeric chain and thereby, enhances the ionic conductivity of the polymer blends and nanocomposites [29]. The T_d values are increased by increasing MWCNTs content, indicating that these fillers improve

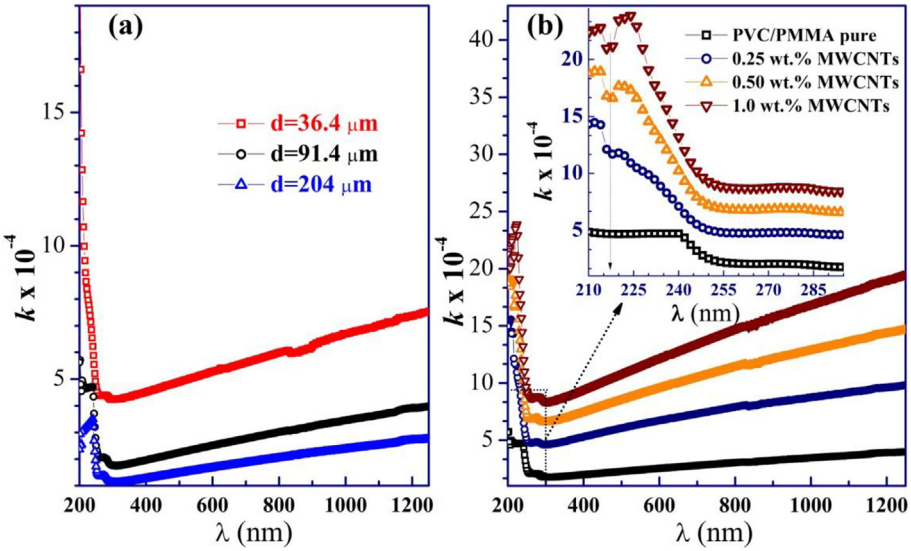

Fig. 6. . the dependence of the absorption index of the films on the wavelength, the inset shows an absorption band at 214 nm for the films loaded with MWCNTs.

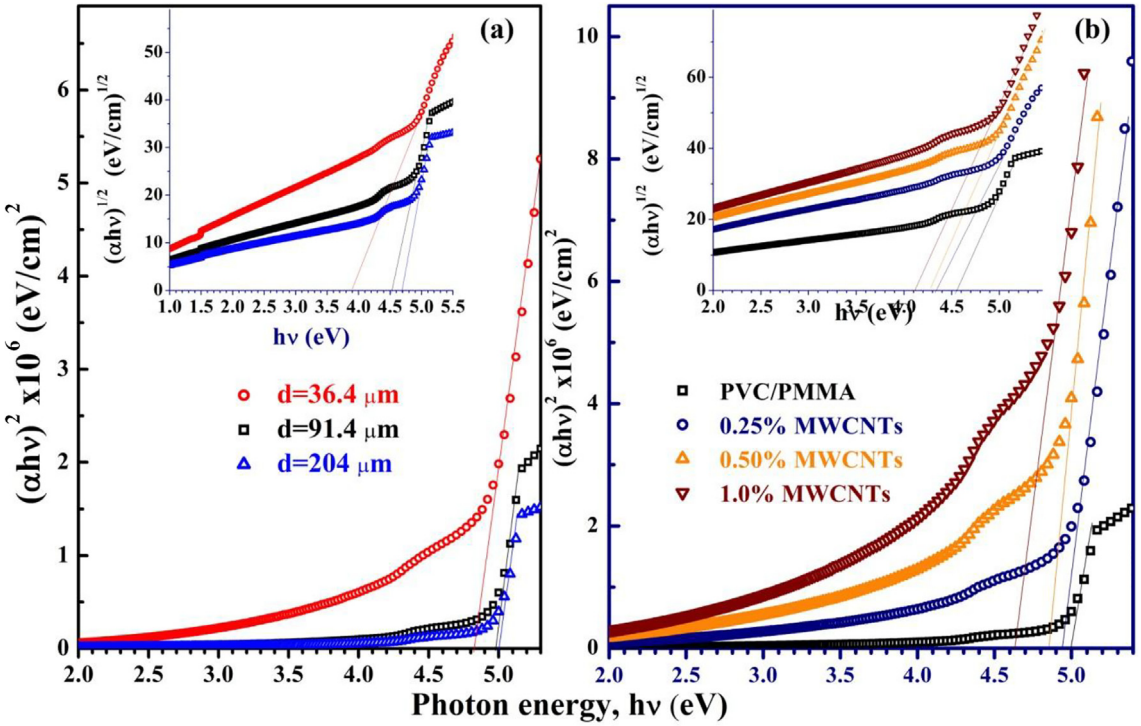

Fig. 7. . Tauc's plots; direct optical band gap (E_g^{di}) of the films and the insets show the indirect optical band gap (E_g^{in}).

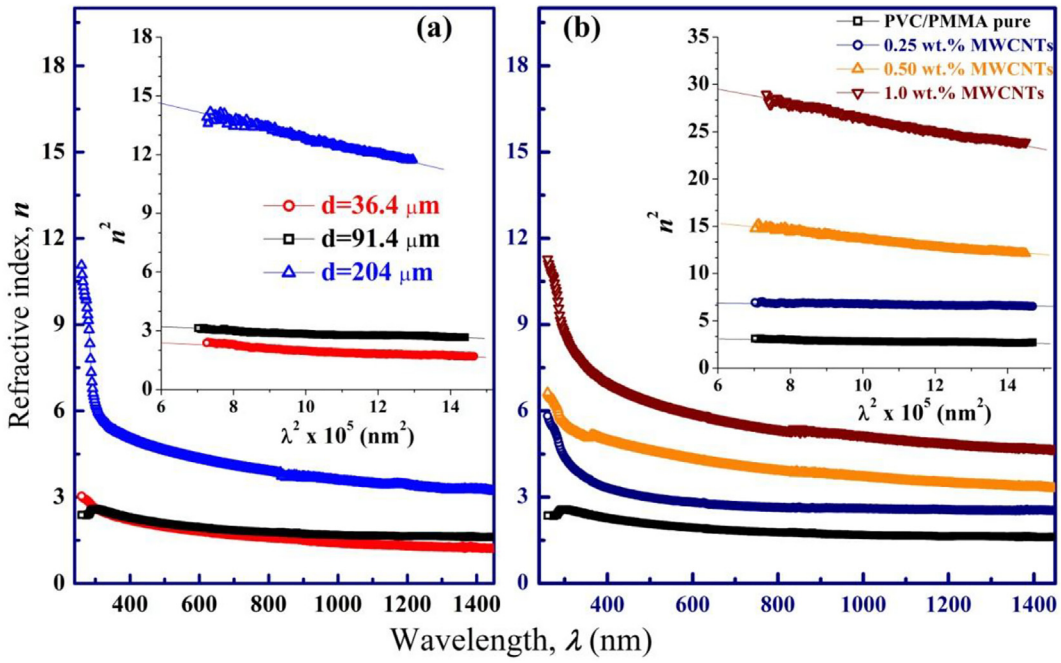

Fig. 8. . The refractive index (n) distribution of the films w.r.t λ. The insets show (n^2 & λ^2) for determination the lattice dielectric constant and charge carriers to electron effective mass ratio of the films.

the thermal stability of the blend [35]. The degree of crystallinity of the blends is calculated using the formula [36]:

$$X_c(\%) = \frac{\Delta H_m}{\Delta H_m^o} \times 100 \quad (1)$$

where ΔH_m is the heat of fusion at T_m and ΔH_m^o is the heat of fusion of 100% crystalline PVC (176 J/g [37]). The values of ΔH_m and X_c (%) are listed in Table 2. The obtained results demonstrate that X_c increases with increasing the film thickness, but decreases with increasing MWCNTs loading from 0.25 to 1.0 wt%. This is owing to the homogenous distribution of the fillers inside the blend matrix. For PVC (60%)/PMMA (40%) blend loaded with NiO NPs, the reported T_g and T_m in the range 80–95 °C and 230–265 °C, respectively. However, at doping ratios >2.0 wt%, the NiO NPs agglomeration yielded an increase in the calculated X_c from ~ 10.63 to 29.26% [19]. The obtained TGA, DTG, and DSC indicate that the thermal properties and stability of P (VC/MMA) blends are adjustable by controlling the films' thickness and MWCNTs doped ratio. Additionally, these materials can be used

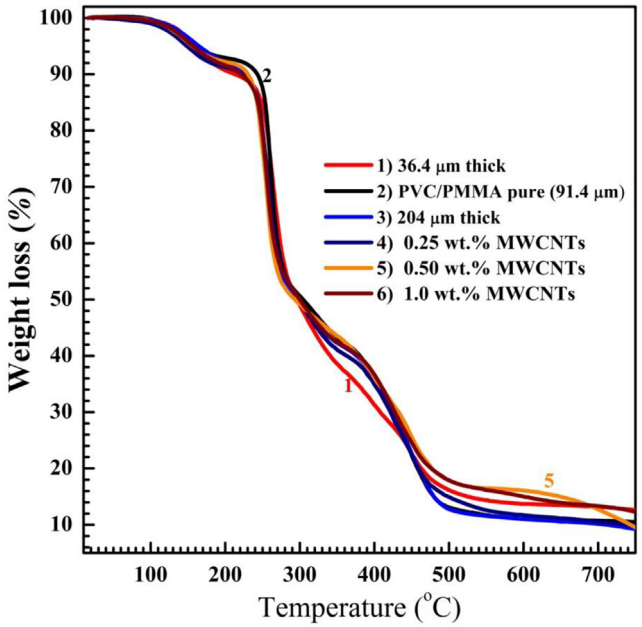

Fig. 9. . TGA thermograms of PVC/PMMA blends of different thickness and that loaded with different ratios of MWCNTs.

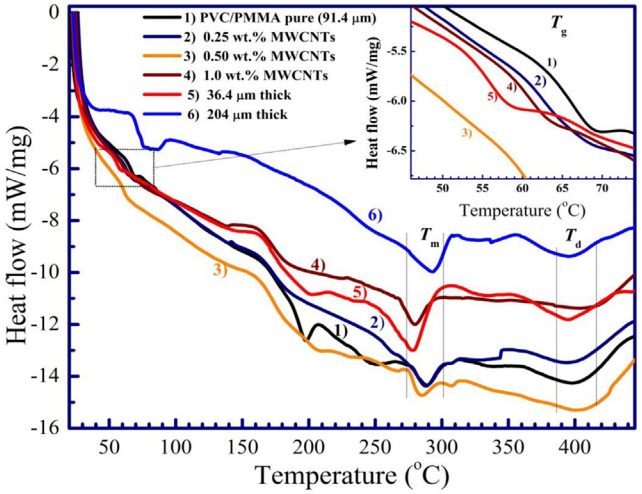

Fig. 10. . DSC curves of PVC/PMMA pure blends of 36.4–204 μm thick, and that loaded with 0.25–1.0 wt% MWCNTs.

efficaciously in microelectronic industry, electronic devices, electromagnetic shielding and space applications without damaging up to 230 °C.

Dielectric properties

Dielectric constant, dielectric moduli, and conductivity

Fig. 11(a, b) shows the variation of the real part of dielectric constant ε' and the loss tangent tan $\delta = \varepsilon''/\varepsilon'$ [38], (the ratio of the electric energy lost to the energy stored in an applied electric field), where ε'' is the dielectric loss. As seen in Fig. 11 (a), ε' values are higher at the very low applied frequency *f*. This is arising from the orientation of P(VC/MMA) polar groups and the charges accumulated at the electrode-film interface [39]. Increasing the film's thickness from 36.4 μm to 204 μm had a small influence on increasing ε' at the low-*f* region, compared to the influence of CNTs loading. For comparison, the ε' values at 10 kHz for all films are listed in Table 3. MWCNTs incorporation may encourage the blend functional groups to have an ordered state and thus causing improvement in the polarization. Increasing the applied *f* values means increasing the reversal of the applied electric field. This causes a decrease in charge carriers' density at electrode-film interface and decreases the orientation of dipoles. This is due to the lag between the frequency of oscillating dipoles and the applied field. This results in decreasing the polarization and ε' and weakens the dipoles' interaction with the electric field [40]. Similar behavior is seen for the dependence of tan δ of the applied *f*. However, the blend loaded with 0.50 wt% MWCNTs shows a relaxation peak shifted to a higher *f* after increasing fillers content to 1.0 wt%. The presence of these peaks is attributed to the conductivity relaxation phenomena, where after this peak, the charge carriers become confined to potential wells and their motion is restricted for short distances. In general, the low-*f* tan δ is greater than that at high *f*. The reason is that as the applied *f* increases, the interfacial polarization decreases and becomes vanishing small that owing to the limited time for the dipoles to orient in the ac electric field direction [41].

Fig. 12 (a, b) shows the dependence of the real (*M′*) and imaginary (*M″*) dielectric moduli of the prepared films on the applied *f*. The very low values of *M′* and *M″* at the low *f* values reveal that the effect of polarization at the electrode/film interface is insignificant and related to a long-range mobility of the charge carriers [42]. The long tail in *M′* and *M″* at the lower *f* values for the 1.0 wt% CNTs loaded film indicates the higher capacitance associated with the electrodes [40]. *M″* increases with increasing *f* at first, owing to the long-range random hopping of charges that reaches to a maximum value at a certain *f* value. The peaks observed in the spectra of *M″* or the relaxation attributed to the change from long-range motion into restricted or caged motion. The *f* value corresponds to the peak is the same for all P(VC/MMA) pure films, regardless of their thickness. However, it shifts to higher values with increasing CNTs loading ratio inside the blend. Further increase in *f*, the values of *M″* decrease, and this indicates that the charge carriers become confined within the potential well and only a short distance move is alloyed. At low *f*, many types of interface states with different lifetimes are available, but these states affected by the applied signal [41]. At higher *f* values, *M″* reaches a nearly constant value. The shift of M''_{max} peak position towards higher *f* after loading the CNTs indicates that increasing CNTs ratio improves and supports the movement of the charge carriers by building up a conductive 3D network throughout the blend matrix.

The total conductivity in a dielectric material is determined from the relation; $\sigma_t = \sigma_{dc} + \sigma_{ac}(f)$, where σ_{dc} is the conductivity at very low or zero frequency, i.e. the limiting zero-frequency conductivity, and the

Table 2
Thermal Properties; the maximum thermal degradation temp. (T_{max}), glass transition temp. (T_g), melting (T_m) and decomposition (T_d) temps., the heat of fusion (ΔH_m) and crystallinity (X_c).

Films		T_{max} (°C)	T_g (°C)	T_m (°C)	T_d (°C)	H_m (J/g)	Xc (%)
Thickness effect	d = 36.4 μm	262	55.0	279	394	33.4	18.97
	d = 91.4 μm	262	64.0	289	400	42.3	24.03
	d = 204 μm	252	70.0	292	395	47.6	27.04
Doping effect	0.25% MWCNTs	258	61.0	289	392	42.5	24.15
	0.50% MWCNTs	259	59.0	285	402	39.7	22.55
	1.0% MWCNTs	261	59.3	280	404	36.8	20.90

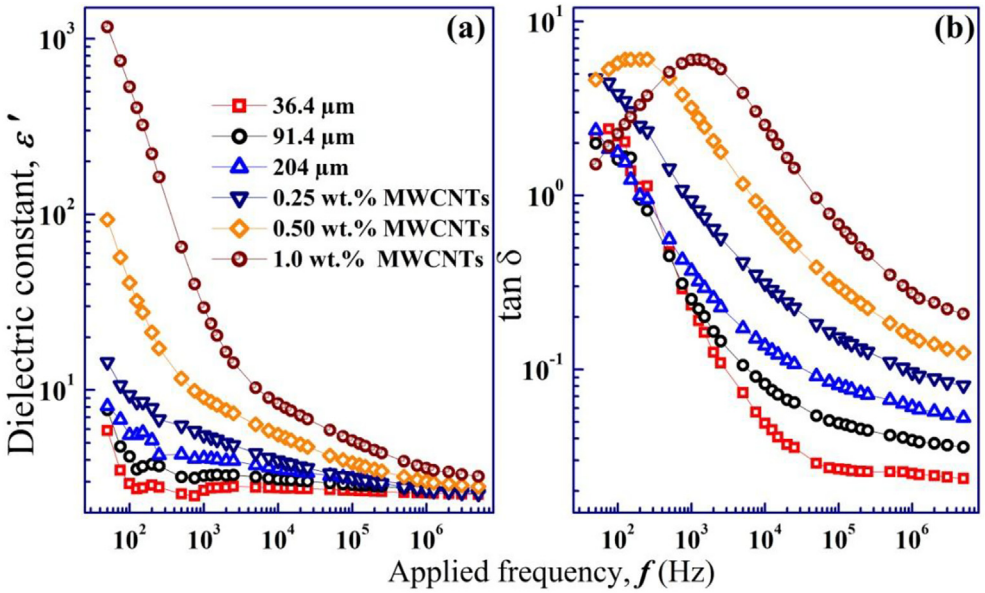

Fig. 11. (a) Dielectric constant (ε') and (b) dielectric loss factor (tan δ) distribution *w.r.t.* the applied frequency of PVC/PMMA blends and nanocomposites.

Table 3
Dielectric properties; dielectric constant at 10 kHz, conductivity at $f = 0$, (σ_{dc}), conductivity at 1 MHz.

Films		ε' at 10 kHz	σ_{dc} (S/m)	σ_{ac} (S/m) at $f = 1$ MHz
Thickness effect	d = 36.4 µm	2.77	3.51×10^{-8}	3.62×10^{-6}
	d = 91.4 µm	3.10	3.83×10^{-8}	5.92×10^{-6}
	d = 204 µm	3.55	5.24×10^{-8}	9.65×10^{-6}
Doping effect	0.25% MWCNTs	3.97	1.96×10^{-7}	1.44×10^{-5}
	0.50% MWCNTs	5.57	1.39×10^{-6}	2.59×10^{-5}
	1.0% MWCNTs	8.37	9.25×10^{-6}	5.48×10^{-5}

ac conductivity; $\sigma_{ac}(f) = 2\pi f \varepsilon_o \varepsilon''$ [42], where ε_o is the permittivity of free space [43]. Fig. 13 shows the σ_{ac} of the samples under study, where their value at the studied f range is $10^{-4}\left(\frac{S}{m}\right) < \sigma_{ac} < 10^{-7}\left(\frac{S}{m}\right)$. In the high f region, the σ_{ac} raises linearly with f, which is ascribed to increasing the mobility of charge carriers [44]. The σ_{ac} values at $f = 1$ MHz are listed in Table 3, where σ_{ac} increases from 3.62×10^{-6} to 9.65×10^{-6} S/m with increasing film thickness and significantly increased to 5.48×10^{-5} S/m after loading 1.0 wt% MWCNTs. The σ_{dc} value was calculated by extrapolating the plateau regions to the Log σ_{ac} axis and measuring the intersections at $f = 0$. This is indicated by the dashed lines in Fig. 13, and the obtained values are listed in Table 3. Ramesh et al. [40] achieved an ionic conductivity in the order of 1.11 x10^{-6} S/cm at RT for P(VC/MMA) mixed with lithium bis (trifluoromethanesulfonyl) imide at the blend/salt ratio of 70/30. However, at such high salt concentrations, the composite films sever from the phase separation. As mentioned in the previous section, T_g of the neat blend had reduced from 64 °C to 59.3 °C for blend loaded with 1.0 wt% MWCNTs. This decrease in T_g indicates the softening of the polymer blend backbone that enhances the flexibility of the polymer backbone and hence increases its σ_{ac}.

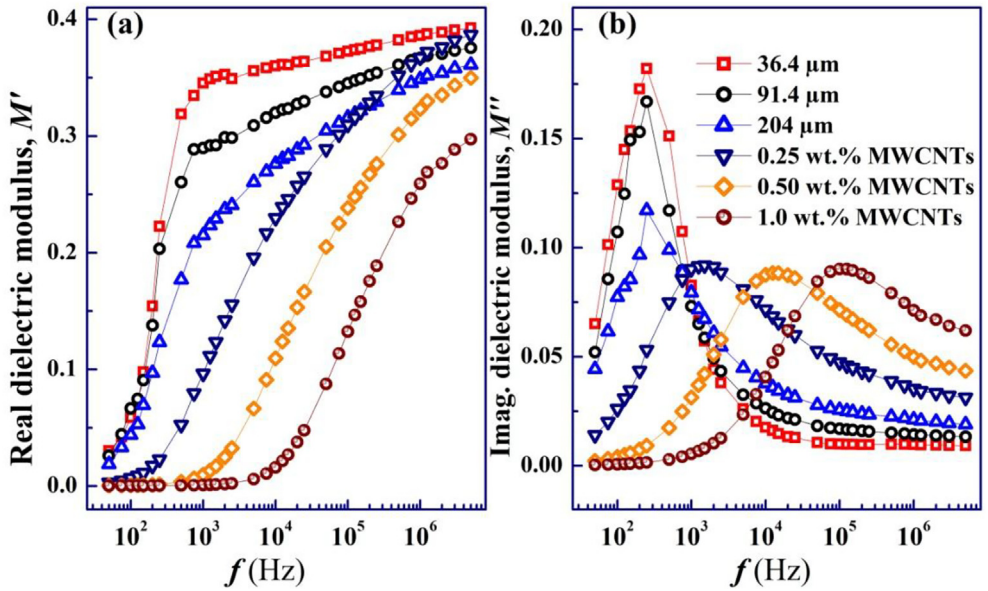

Fig. 12. . Variation of (a) the real and (b) the imaginary part of dielectric modulus (M', M'') for PVC/PMMA films with different thickness or loaded with 0.25, 0.50, and 1.0 wt% MWCNTs.

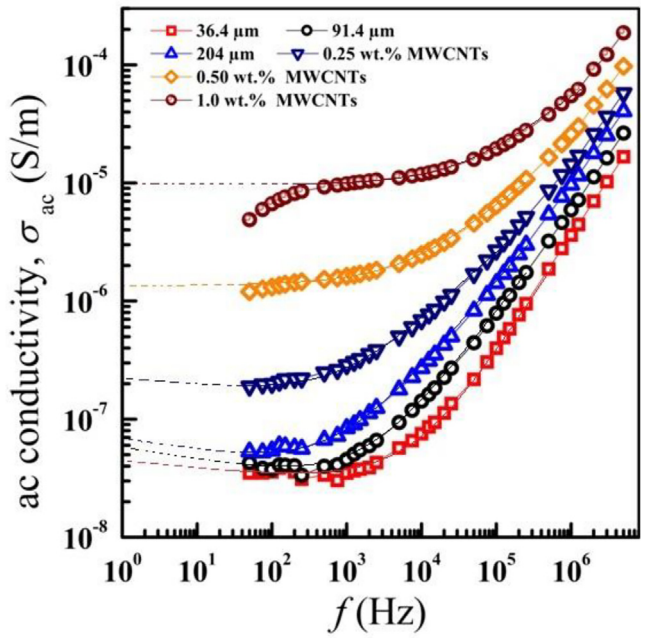

Fig. 13. . ac conductivity of the films in the frequency rang $f = 50$ Hz- 5 MHz. Dashed lines show the DC conductivity ($f = 0$).

Impedance spectroscopy

The complex impedance is defined as: $Z^* = Z^{'} + iZ^{''}$, and the real Z' and imaginary Z'' parts are related to ε' and ε'' by the equations [14]:

$$\varepsilon'(\omega) = \frac{Z^{''}}{\omega C_o (Z'^2 + Z''^2)}, \varepsilon''(\omega) = \frac{Z'}{\omega C_o (Z'^2 + Z''^2)}, \quad (2)$$

where $C_o = (\varepsilon_o A)/d$, and A is the electrode-film contact area. Z' gives the information about the resistive part, while Z'' gives the reactance part arising due to the capacitive and inductive nature of the system. Fig. 14 (a, b) illustrates the dependence of Z' and Z'' of the P(VC/MMA) films on the applied f at RT. As mentioned, ε' decreases with f and also Z' decreases with increasing f. However, the values of Z' decrease slightly till a certain value of f, depending on the films' composition. Then, decrease sharply with a further increase in f. At lower f side, Z' values decrease slightly with increasing film thickness but significantly decrease with increasing MWCNTs content creating a plateau region extend to about 10^4 Hz for P(VC/MMA)/1.0% MWCNTs composite. The observed shift of Z' plateau for the nanocomposite films confirms the existence of a frequency relaxation process in these composites. Inserting CNTs among the blend chains enhances the process of space charge releasing [39,45]. At higher frequencies, the role of the interfacial polarization is limited and the Z' value of the films be comparable [39]. Additionally, Z'' & f exhibits a similar trend, Fig. 14 (b), with a wave-like behavior at the lower f region. The observed lowering in the peaks' position in Z'' spectra with increasing CNTs ratio is arising from the creation of extra conductive networks and pathways for ions movement in the blend. Moreover, in the high-f region, the values of Z'' tend merging. This may be due to the accumulation of space charge in the blend matrix [45]. These results and according to Fig. 13 and Fig. 14 (a, b), the inverse proportionality between Z' and σ_{ac} is confirmed. The formation of the conductive channels is affected by the uniform distribution of the MWCNTs, as seen in Fig. 3 (b-d). Through these inter-connected conductive channels, the electron can easily tunnel which is the main cause for the reduction of Z'.

Fig. 15(a–d) shows the Col-Cole plots for all samples. For P(VC/MMA) blends, Z' vs. Z'' relation exhibits slanted straight lines regardless of the film's thickness. However, the plot become in the form of a semicircle after loading the blend with 0.25 wt% MWCNTs. With increasing fillers ratio to 0.5 and 1.0 wt%, a slanted spike at the lower frequencies has appeared with a semicircle at high frequency. The slanted spike is due to the polarization effect at the electrode-film interface and indicates to a non-ideal mode of capacitance behavior in the nanocomposites. The semicircle portion is expressed by a parallel combination of bulk capacitance (due to the immobile polymer chains) and bulk resistance (because of ions migration) as shown in the insets of Fig. 15 (b, d). The absence of semicircles in Fig. 15 (a) indicates the random dipole orientation in the blend's side chains as well as the non-capacitance nature [40]. Additionally, the spike is elongated and the semicircle diameter is decreased with increasing MWCNTs content from 0.5 to 1.0 wt%. The decrease in the area under the semicircle again confirms the increase in bulk capacitance of the material with an

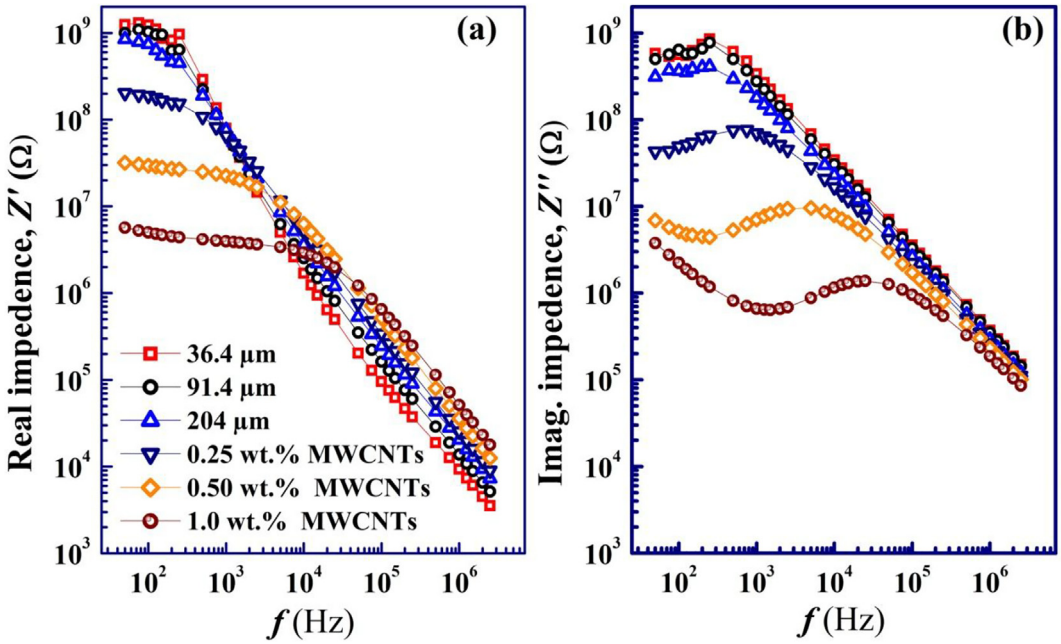

Fig. 14. . The dependence of (a) the real and (b) the imaginary part of impedance for PVC/PMMA films with different thickness or loaded with 0.25, 0.50, and 1.0 wt % MWCNTs.

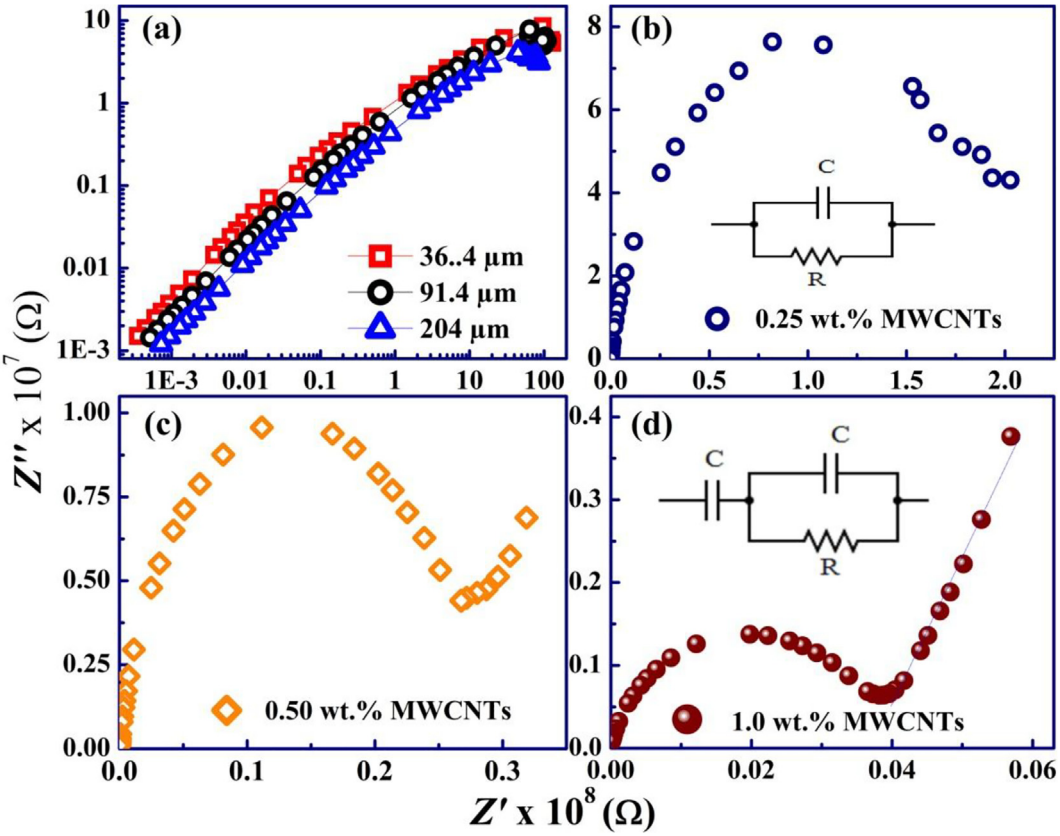

Fig. 15. . Cole-Cole (Nyquist) plots of the PVC/PMMA loaded with (a) 0.25 wt%., (b) 0.50 wt%., and (c) 1.0 wt% MWCNTs. (a') and (b') are the equivalent circuits for (a) and (b,c), respectively.

increase in MWCNT loading. This behavior is due to the uniform dispersion of the fillers that form interconnected network structures inside P(VC/MMA) blend matrix [3].

Conclusion

Blends and nanocomposite films based on P(VC/MMA)/MWCNTs were successfully prepared by a solution casting technique. The influences of film thickness and MWCNTs doping ratio on the morphological, molecular vibration, optical, thermal and dielectric properties were investigated. SEM analysis showed that the blend films exhibit a net-wrinkle or fingerprint-like structure turned to be a wave-like morphology after MWCNTs loading. FTIR spectra showed that no peaks shift with increasing film thickness or MWCNTs content. Besides the overlapping between the functional groups of both PVC and PMMA, the interactions between the components of blends and nanocomposites improved the peaks intensity of C—H and C═O. The UV–vis transmittance was decreased with increasing film thickness from 36.4 to 204 µm and also decreased after MWCNTs loading. Both E_g^{di} and the refractive index were increased from 4.82 to 5.0 eV and from 1.8 to 3.6 with increasing P(VC/MMA) blend thickness. Additionally, E_g^{di} was decreased from 5.0 to 4.63 eV after doping with 1.0 wt% MWCNTs. TGA showed that all have thermal stability between 179 and 230 °C. The maximum thermal degradation temp. (T_{max}), decreased from 262 to 252 °C with increasing the film's thickness. Also, its values are in the range 255–261 °C, after loading with MWCNTs. DSC thermograms showed that the melting temperature (T_m) and the degree of crystallinity (X_c) increased from 279 to 292 °C and 18.97 to 27.04% with increasing the thickness. These values decreased from 289 to 280 °C and from 24.03 to 20.90% due to the homogenous distribution of MWCNTs inside the blend. All films showed $10^{-4}\left(\frac{S}{m}\right) < \sigma_{ac} < 10^{-7}(\frac{S}{m})$. σ_{dc} and σ_{ac} (at 1 MHz) increases from 3.51 to 5.24 × 10^{-8} S/m and 3.62 × 10^{-6} to 9.65 × 10^{-6} S/m, respectively, with increasing film thickness. Also, they increased significantly 9.25 × 10^{-6} and 5.48 × 10^{-5} S/m, respectively, after loading 1.0 wt% MWCNTs. The impedance spectroscopy confirmed the inverse proportional between Z' and σ_{ac}. Nyquist plots showed slanted straight lines for pure blends and slanted spikes at the lower frequencies combined with semicircles at high frequency for the blend loaded with 0.5 and 1.0 wt% MWCNTs. Introducing MWCNTs induce a capacitance nature for the blend. In summary, the optical, thermal and dielectric properties of P(VC/MMA) blend are adjustable by modifying its thickness and MWCNTs filled ratio. In summary, the obtained results illustrate that the prepared films are a candidate for designing high refractive index lenses or optical filters with a reasonable optical bandgap. The observed thermal stability and enhanced electric conductivity make the materials suitable for electromagnetic shielding and space applications up to temperatures of 230 °C. The improved dielectric constant and the induced capacitance nature after MWCNTs loading pave the way for use in the microelectronic industry, integral thin film capacitors and electric stress control devices.

A statement of the novelty

This research paper presents a simple and an effective methods for controlling the physical properties of a thermoplastic polymeric blend, PVC/PMMA, which is multifunctional material. This was done by varying the film thickness (36.4 to 204 µm). The film of thickness that gave the best physical properties, was then doped by MWCNTs with different ratios.

Few reports on PVC/PMMA/MWCNTs are found. No reports are found on the thickness effect on the blend properties. Therefore, this is the first complete study which is devoted to explain how to manipulate the structural, optical, thermal, electric properties and capacitance

behavior of P(VC-MMA)/MWCNTs nanocomposite films.

Declaration of Competing Interest

The authors declare that they have no known competing financial interests or personal relationships that could have appeared to influence the work reported in this paper.

Appendix A. Supplementary data

Supplementary data to this article can be found online at https://doi.org/10.1016/j.rinp.2020.103025.

References

[1] Alghunaim NS. Structural, thermal, dielectric spectroscopic and AC impedance properties of SiC nanoparticles doped PVK/PVC blend. Res Phys 2018;9:1136–40.
[2] Shakir MF, Khan AN, Khan R, Javed S, Tariq A, Azeem M, et al. EMI shielding properties of polymer blends with inclusion of graphene nano platelets. Res Phys 2019;14:102365.
[3] Hota NK, Karna N, Dubey KA, Tripathy DK, Sahoo BP. Effect of temperature and electron beam irradiation on the dielectric properties and electromagnetic interference shielding effectiveness of ethylene acrylic elastomer/millable polyurethane/SWCNT nanocomposites. Eur Polym J 2019;112:754–65.
[4] Aziz SB, Abdullah OG, Brza MA, Azawy AK, Tahir DA. Effect of carbon nano-dots (CNDs) on structural and optical properties of PMMA polymer composite. Res. Phys. 2019;15:102776.
[5] Suresh SS, Mohanty S, Nayak SK. Preparation and characterization of recycled blends using poly(vinyl chloride) and poly(methyl methacrylate) recovered from waste electrical and electronic equipments. J Clean Prod 2017;149:863–73.
[6] Joseph J, Deshmukh K, Chidambaram K, Faisal M, Selvarajan E, Sadasivuni KK, et al. Dielectric and electromagnetic interference shielding properties of germanium dioxide nanoparticle reinforced poly(vinyl chloride) and poly(methylmethacrylate) blend nanocomposites. J Mater Sci: Mater Electron 2018;29(23):20172–88.
[7] Arunkumar R, Babu RS, Rani MU, Kalainathan S. Effect of PBMA on PVC-based polymer blend electrolytes. J Appl Polym Sci 2017;134:44939.
[8] Feng A, Wu G, Wang Y, Pan C. Synthesis, preparation and mechanical property of wood fiber-reinforced Poly(vinyl chloride) composites. J Nanosci Nanotechnol 2017;17:3859–63.
[9] Mohammed Gh, El Sayed AM, El-Gamal S. Effect of M nitrates on the optical, dielectric relaxation and porosity of PVC/PMMA membranes (M = Cd Co, Cr or Mg). J Inorg Organomet Polym Mater 2019. https://doi.org/10.1007/s10904-019-01307-9.
[10] Kim K-I, Kim D-A, Patel KD, Shin US, Kim H-W, Lee J-H, et al. Carbon nanotube incorporation in PMMA to prevent microbial adhesion. Sci Rep 2019;9:4921.
[11] Fu Q, Lin G, Chen X, Yu Z, Yang R, Li M, et al. Mechanically reinforced PVdF/PMMA/SiO_2 composite membrane and its electrochemical properties as a separator in lithium-ion Batteries. Energy Technol 2018;6:144–52.
[12] Kim DH, Park MS, Cho HH, Park JT, Kim JH. Synthesis of organized mesoporous metal oxide films templated by amphiphilic PVA–PMMA comb copolymer. RSC Adv 2016;6:67849.
[13] Bhran A, Shoaib A, Elsadeq D, El-gendi A, Abdallah H. Preparation of PVC/PVP composite polymer membranes via phase inversion process for water treatment purposes. Chin J Chem Eng 2018;26:715–22.
[14] Prasanna CMS, Suthanthiraraj SA. Dielectric, thermal, and electrochemical properties of PVC/PEMA blended polymer electrolytes complexed with zinc triflate salt. Ionics 2017;23:3137–50.
[15] Elashmawi IS, Alatawi NS, Elsayed NH. Preparation and characterization of polymer nanocomposites based on PVDF/PVC doped with graphene nanoparticles. Res Phys 2017;7:636–40.
[16] Cui J-Y, Cai Y-B, Yuan W-J, Lv Z-F, Zhang C, Xu S-A. Preparation of PMMA grafted calcium carbonate whiskers and its reinforcement effect in PVC. Polym Compos 2017;38:2753–61.
[17] Arunkumar R, Babu RS, Rani MU. Investigation on Al2O3 doped PVC–PBMA blend polymer electrolytes. J Mater Sci: Mater Electron 2017;28:3309–16.
[18] Mzir T, Khemici MW, Dahmane M, Mzir M, Doulache N. Dielectric characterization of polyvinyl chloride/polymethyl methacrylate (PVC/PMMA) blends by TSDC technique. Int J Polym Anal Charac 2018;23(8):675–83.
[19] Khutia M, Joshi GM. Dielectric relaxation of PVC/PMMA/NiO blends as a function of DC bias. J Mater Sci Mater Electron 2015;26:5475.
[20] Wang N, Wu X, Liu CS. Opposite Effects of SiO2 Nanoparticles on the Local α and Larger-Scale α' Segmental Relaxation Dynamics of PMMA Nanocomposites. Polymers 2019;11:979.
[21] Chuayjuljit S, Neeranatmanit K, Boonmahitthisud A. Property improvement of plasticized Poly(vinyl chloride) by Nano-TiO_2 and Poly(methyl methacrylate)–Encapsulated Nano-TiO_2. J Vinyl Addit Technol 2016;22:433–40.
[22] Ayaz S, Ishaq M, Saeed K, Ahmed I, Khalil NK. Investigation of thermal, mechanical and electrochemical properties of nanocomposites based on CuO modified Poly (vinyl chloride)/Poly(methyl methacrylate) blend. J Vinyl Addit Technol 2017;23:80–5.
[23] Ma W, Zhao Y, Li Y, Zhang P, Cao Z, Yang H, et al. Synthesis of hydrophilic carbon nanotubes by grafting poly(methyl methacrylate) via click reaction and its effect on poly(vinylidene fluoride)-carbon nanotube composite membrane properties. Appl Surf Sci 2018;435:79–90.
[24] Zidan HM, Abdelrazek EM, Abdelghany AM, Tarabiah AE. Characterization and some physical studies of PVA/PVP filled with MWCNTs. J.Mater Res Technol 2019;8(1):904–13.
[25] Ryu SH, Cho H-B, Kim S, Kwon Y-T, Lee J, Park K-R, et al. The effect of polymer particle size on three-dimensional percolation in coreshell networks of PMMA/MWCNTs nanocomposites: properties and mathematical percolation model. Compos Sci Technol 2018;165:1–8.
[26] Kumar A, Kumar V, Kumar M, Awasthi K. Synthesis and characterization of hybrid PANI/MWCNT nanocomposites for EMI applications. Polym Compos 2019;39(11):3858–68.
[27] Wu G, Jia Z, Zhou X, Nie G, Lv H. Interlayer controllable of hierarchical MWCNTs@C@Fe_xO_y cross-linked composite with wideband electromagnetic absorption performance. Compos A Appl Sci Manuf 2020;128:105687.
[28] Abdelrazek EM, Elashmawi IS, Hezma AM, Rajeh A. Mustafa Kamal, Effect of an encapsulate carbon nanotubes (CNTs) on structural and electrical properties of PU/PVC nanocomposites. Phys B 2016;502:48–55.
[29] Mahant YP, Kondawar SB, Nandanwar DV, Koinkar P. Poly(methyl methacrylate) reinforced poly(vinylidene fluoride) composites electrospun nanofibrous polymer electrolytes as potential separator for lithium ion batteries. Mater Renew Sustain Energy 2018;7:5.
[30] Khmissi H, El Sayed AM, Shaban M. Structural, morphological, optical properties and wettability of spin-coated copper oxide; influences of film thickness, Ni, and (La, Ni) co-doping. J Mater Sci 2016;51:5924–38.
[31] Yassin AY, Mohamed A, Abdelrazek EM, Morsi MA, Abdelghany AM. Structural investigation and enhancement of optical, electrical and thermal properties of poly (vinyl chloride-co-vinyl acetate-co-2-hydroxypropyl acrylate)/graphene oxide nanocomposites. J Mater Res Technol 2019;8(1):1111–20.
[32] Mohammed MI. Optical properties of ZnO nanoparticles dispersed in PMMA/PVDF blend. J Molec Struct 2018;1169:9–17.
[33] El Sayed AM, Shaban M. Morphological, surface and optical properties of spin-coated IrOx films; influence of spin speed, annealing and (Cr, La) codoping. Ceram Int 2019;45:8460–70.
[34] Abdelghany AM, Abdelrazek EM, ElShahawy A, Al- Muntaser AA. FTIR and UV/Vis. spectroscopy: a key for miscibility investigation of PVC/PMMA polymer blend Middle East. J Appl Sci 2015;5:36–44.
[35] Alghunaim NS. Spectroscopic analysis of PMMA/PVC blends containing $CoCl_2$. Res Phys 2015;5:331–6.
[36] Hassen A, El Sayed AM, Morsi WM, El-Sayed S. Influence of Cr2O3 nanoparticles on the physical properties of polyvinyl alcohol. J Appl Phys 2012;112:093525.
[37] Roger L. Blaine, TA Instruments, 109 Lukens Drive, New Castle DE 19720, USA.
[38] Feng A, Ma M, Jia Z, Zhang M, Wu G. Fabrication of $NiFe_2O_4$@carbon fiber coated with phytic acid-doped polyaniline composite and its application as an electromagnetic wave absorber. RSC Adv 2019;9:25932.
[39] Verma ML, Sahu HD. Study on ionic conductivity and dielectric properties of PEO-based solid nanocomposite polymer electrolytes. Ionics 2017;23(9):2339–50.
[40] Ramesh S, Liew C-W, Ramesh K. Ionic Conductivity, Dielectric Behavior, and HATR–FTIR Analysis onto Poly(methyl methacrylate)–Poly(vinyl chloride) Binary Solid Polymer Blend Electrolytes. J Appl Polym Sci 2013;127(4):2380–8.
[41] Sevgili Ö, Taşçıoğlu İ, Boughdachi S, Azizian-Kalandaragh Y, Altındal Ş. Examination of dielectric response of Au/HgS-PVA/n-Si (MPS) structure by impedance spectroscopy method. Phys B 2019;566:125–35.
[42] Alptekin S, Tataroglu A, Altındal Ş. Dielectric, modulus and conductivity studies of Au/PVP/n-Si (MPS) structure in the wide range of frequency and voltage at room temperature". J Mater Sci Mat Electron 2019;30:6853–9.
[43] El-Sayed S, El Sayed Adel M. Synthesis characterisation, dielectric, and optical properties of the chitosan/poly(ethylene glycol)/magnesia biopolymer nanocomposites. Mater Technol 2019;34(10):602–14.
[44] Hemalatha K, Sriprakash G, Prasad MA, Damle R, Rukmani K. Temperature dependent dielectric and conductivity studies of polyvinyl alcohol-ZnO nanocomposite films by impedance spectroscopy. J Appl Phys 2015;118:154103.
[45] Abdelrazek EM, Abdelghany AM, Tarabiah AE, Zidan5 HM. AC conductivity and dielectric characteristics of PVA/PVP nanocomposite filled with MWCNTs. J Mater Sci Mat Electron 2019;30:15521–33.